JGISE Vol. 9 No. 1 (2026), pp. 108 - 115 | https://doi.org/10.22146/jgise.107851

JGISE

Journal of Geospatial Information Science and Engineering

ISSN: 2623-1182 | https://jurnal.ugm.ac.id/jgise

Decomposition of Postseismic Signals Following ≥Mw 6 Earthquakes on Sumatra Island Based on Sumatran GPS Array (SuGAr) Observations

Tattyana Wening Kalbuadi[1,2], Nurrohmat Widjajanti[2], Cecep Pratama[2]

[1]Badan Informasi Geospasial, Indonesia

[2]Departemen Teknik Geodesi, Fakultas Teknik, Universitas Gadjah Mada, Indonesia

Correspondent Author: Nurrohmat Widjajanti| **Email:** nwidjajanti@ugm.ac.id

Diterima (*Received*): 12/Jun/2025 Direvisi (*Revised*): 09/May/2026 Diterima untuk Publikasi (*Accepted*): 19/May/2026

ABSTRACT

Indonesia, located at the convergence of four major tectonic plates, experiences frequent large earthquakes, particularly in Sumatra, due to the subduction of the Indo-Australian Plate and the Sumatra Fault Zone (SFZ). While most postseismic studies focus on events with magnitudes ≥7 Mw, this research investigates earthquakes with magnitudes ≥6 Mw to characterize postseismic deformation on Sumatra Island. Using SuGAr GPS time series data from 2002 to 2023, postseismic signals were decomposed and modelled using an exponential decay function to isolate transient deformation and estimate decay time parameters. Model performance was evaluated through RMSE comparisons and two-parameter significance tests at the 95% confidence level. The results indicate consistent RMSE patterns in the NS and EW components, whereas the UD component shows greater variability, suggesting that the model effectively captures horizontal postseismic motion but is less sensitive to vertical displacement.

Keywords: *Time Series, SuGAr GPS, Postseismic, Exponential*

1. Introduction

Indonesia is located in one of the most active seismic regions in Southeast Asia, bordered by four major tectonic plates: the Eurasian, Indo-Australian, Pacific, and Philippine Sea Plates. This tectonic interaction makes the region, particularly Sumatra Island, highly vulnerable to large earthquakes. Sumatra's seismicity is primarily controlled by the subduction of the Indo-Australian Plate beneath the Eurasian Plate and by strike-slip movement along the SFZ, which extends along the Bukit Barisan Mountain range. The oblique subduction off the western coast occurs at a rate of 5–6 cm/year (DeMets et al., 2010), increasing the likelihood of frequent and destructive earthquakes.

Several large earthquakes have struck Sumatra, including the devastating 2004 Aceh earthquake (9.2 Mw), followed by major events in 2009 (Padang) and 2010 (Mentawai) (Heliani et al. 2025). Data from the Advanced National Seismic System (ANSS) indicate that over the past four decades, the region has experienced 11 earthquakes of ≥7 Mw and 65 of ≥6 Mw. Despite this frequency, most previous postseismic studies have focused only on events ≥7 Mw, often with short observational periods and limited data.

Past research using GNSS data from networks like SuGAr and Ina-CORS (Feng et al., 2015; Pratama et al., 2020) applied logarithmic and exponential models to estimate postseismic decay times but often overlooked smaller-magnitude events and seasonal effects. Pratama et al. (2019) estimate the impact of both large and small-to-intermediate magnitude earthquakes (<6 Mw) on the geodetic reference frame. The findings highlight that while large earthquakes contribute significantly to displacement, the cumulative effect of smaller events is also significant, particularly in tectonically active regions such as Sumatra, West Java, and Palu. However, many of these studies did not account for smaller-magnitude events or seasonal effects, limiting the applicability of their findings to current seismic trends.

The coseismic phase represents sudden crustal displacement occurring during an earthquake, while the postseismic phase reflects the gradual adjustment of the crust following the mainshock through mechanisms such as afterslip, viscoelastic relaxation, and poroelastic rebound. Studying these phases is essential because postseismic deformation may persist for months to years and significantly influence crustal motion estimates derived from GNSS observations. In tectonically active regions such as Sumatra, understanding postseismic behavior is particularly important for improving deformation models, maintaining geodetic reference frame stability, and providing insight into seismic cycle processes following moderate to large earthquakes.

This study addresses these gaps by focusing on postseismic deformation following ≥6 Mw earthquakes in Sumatra, using long-term GNSS time series data from eight SuGAr stations recorded between 2002 and 2023. By applying exponential modelling, this research aims to improve estimates of decay time and station-displacement velocity. The results are expected to offer a more comprehensive understanding of tectonic deformation in Sumatra and provide updated insights into the region's seismic response based on a broader magnitude range and extended temporal coverage.

2. Data, Methods, and Tools

2.1. Study Area

This research covers Sumatra Island and its surrounding smaller islands. Sumatra is the third-largest island in Indonesia after Kalimantan and Papua. It is located between 5°39' North Latitude (N) and 5°54' South Latitude (S), and 95° East Longitude (E) to 106° East Longitude (E). The Bukit Barisan Mountain range extends north to south across the island (Whitten & Damanik, 2012).

Geographically, Sumatra is divided into two main regions: mountainous areas and lowlands. The mountainous region consists of valleys that form part of the Bukit Barisan range, which bisects Sumatra. West Sumatra Province, traversed by the Bukit Barisan Mountains, features diverse natural resources and several conservation areas (Inger & Voris, 2001).

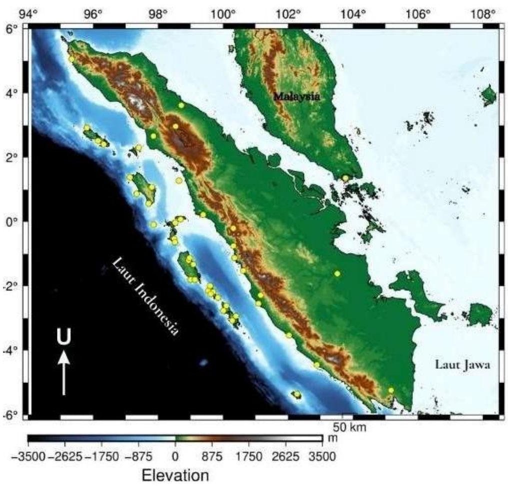

Figure 1. Distribution of SuGAr stations (Feng et al., 2015b)

2.2. Data

The primary dataset used in this study comprises daily GNSS coordinate solutions from eight SuGAr stations spanning 2002 to 2023 (Figure 1). These stations are presented in Table 1. The data are provided in topocentric coordinate components (North-South/NS, East-West/EW, and Up-Down/UD), referenced to epoch 2012 and aligned with the ITRF2014 reference frame. These observational data were obtained from the SuGAr data archive via ftp://ftp.earthobservatory.sg/SugarData.

Table 1. List of SuGAr stations

Station	**Location**
ABGS (Air Bangis)	Sumatera Selatan
BSAT (Bulasat)	Kepulauan Mentawai
BTHL (Batang Hulu)	Sumatera Barat
BUKT (Bukit Tinggi)	Sumatera Barat
JMBI (Jambi)	Jambi
MSAI (Muara Siberut)	Kepulauan Mentawai
NGNG (Nyang Nyang)	Pulau Pagai
PTLO (Pulo Aceh)	Aceh

Table 2. List of earthquake events and magnitudes

Earth quake ID	***Longitude***	***Latitude***	**Magni-tudo (Mw)**
1	0°50'19.68"	98°50'6"	6.1
2	0°8'11.04"	96°38'39.12"	6.7
3	2°20'53.16"	96°21'27"	6.3
4	-2°9'32.4"	99°41'17.16"	6.3
5	4°55'37.2"	95°54'25.2"	6.1
6	1°38'24"	99°8'49.2"	6
7	0°24'54"	97°49'30"	6.1
8	-1°48'29.52"	98°30'40.32"	7.1
9	-4°29'13.2"	100°4'55.2"	7.8
10	2°22'58.8"	97°2'52.8"	7.2
11	2°22'58.8"	97°2'52.8"	7.8
12	-1°43'12"	99°52'1.2"	7.6
13	-3°29'9.6"	99°58'19.2"	7.2
14	-2°7'48"	99°37'37.2"	7.4
15	-3°7'48"	99°37'37.2"	7
16	-5°26'16.8"	101°22'1.2"	7.9
17	-5°51'32.4"	107°25'8.4"	8.4
18	-6°51'32.4"	107°25'8.4"	7.5
19	2°5'6"	97°6'28.8"	8.6
20	3°17'42"	95°58'55.2"	9.1
21	-3°25'37.2"	103°58'516"	7.3
22	2°49'26.4"	96°5'6"	7.4
23	2°49'26.4"	96°5'6"	8.2
24	2°19'37.2"	93°3'46.8"	8.6

In addition to the GNSS time series, earthquake catalog data with magnitudes ≥6 Mw were compiled to investigate postseismic deformation characteristics and decay times associated with moderate-to-large earthquakes in Sumatra. Initially, all recorded earthquakes within the study region during the observation period were considered. However, to minimize overlapping postseismic signals from temporally adjacent earthquakes, only events separated by at least six months from other earthquakes of comparable magnitude were selected.

Based on this filtering process, 24 earthquakes with magnitudes ≥6 Mw were identified and used for further analysis (Table 2). These selected events were analyzed using GNSS observations from the eight SuGAr stations to model postseismic deformation using exponential fitting. The filtering procedure was necessary due to the high frequency of seismic events in Sumatra, which may complicate the isolation of individual postseismic responses (Wu & Wang, 2025).

2.3. Method

To provide a clearer overview of the research workflow. The key stages undertaken in this study are summarized as follows. This methodology follows prior research that emphasizes the effectiveness of exponential decay models in capturing viscoelastic and afterslip-related deformation (Yusiyanti et al., 2023; Yusiyanti et al., 2025). This workflow is designed to provide a comprehensive assessment of crustal deformation using SuGAr observation data.

The methodology of this research began with a comprehensive literature review to understand the theoretical framework surrounding postseismic deformation, GNSS data analysis, and modelling techniques. The necessary tools and materials were prepared, including software and data sources. GNSS observations were obtained from the SuGAr network and processed using the Canadian Spatial Reference System-Precise Point Positioning (CSRS-PPP) method to generate precise daily position solutions. A time series of position changes from 2002 to 2023 was then constructed for each observation point. Simultaneously, earthquake distribution data were collected to evaluate the potential impact on GNSS stations.

Earthquake catalog data with magnitudes ≥6 Mw were collected to identify seismic events that could influence GNSS stations. To reduce overlapping postseismic signals from closely spaced earthquakes, only events separated by at least six months from earthquakes of comparable magnitude were selected. This criterion was adopted because postseismic deformation may persist for several months after a mainshock, potentially interfering with the isolation of individual postseismic responses.

The distance between each earthquake event and observation station was calculated to determine which stations were significantly affected. Stations within the deformation-influence zone that exhibited observable displacement anomalies after the earthquake were selected. The postseismic phase of each selected time series was decomposed and modelled using an exponential decay approach (Model 1). This model enabled the estimation of key parameters, including the Root Mean Square Error (RMSE) and decay time, which reflect the model's accuracy and the temporal characteristics of postseismic displacement. Finally, the results were analyzed to assess the model's effectiveness and to provide physical insights into the postseismic processes observed.

2.3.1 RINEX Data Processing

Raw GNSS data were processed using the PPP method via the Canadian Geodetic Survey's CSRS-PPP service (https://webapp.csrs-scrs.nrcan-rncan.gc.ca/geod/tools-outils/ppp.php). This dual-frequency PPP approach utilizes precise satellite orbit and clock products to determine absolute station positions.

RINEX files underwent quality control with TEQC, then compressed (<300 MB) and uploaded to the CSRS-PPP platform. Processing parameters were configured for the automated correction application and full data access. Output includes position solutions and observation residuals.

Since CSRS-PPP results are referenced to the first epoch of each calendar year, all solutions were epoch-adjusted to a common reference epoch for subsequent analysis.

2.3.2 Postseismic Deformation Parameter Estimation

Postseismic deformation parameters were estimated by fitting mathematical functions to GNSS time series data. An exponential decay function was applied to each observation station's time series components (NS, EW, UD) using the curve fitting toolbox. The output includes estimated model parameters and RMSE values for each component. This approach aims to characterize the postseismic deformation mechanisms associated with each earthquake event. The exponential approach used in this study is expressed by the following equation Feng et al., 2015.

$$P(t_i) = \sum_{j=1}^{n} b_j \left(1 - exp\ \frac{teq_j - t_i}{\tau_j^{log}}\right) H\ (t_i - tq_i) \qquad (1)$$

The equation shown represents the postseismic displacement model $P(t_i)$ which is expressed as a sum of exponential decay functions. Here, b_j is the amplitude of the postseismic signal for the j -th earthquake, teq_j is the occurrence time of the j -th earthquake, τ_j^{log} is the logarithmic decay constant associated with the postseismic response, and $H\ (t_i - tq_i)$ is the Heaviside step function that ensures the model only activates after the earthquake event. The expression models how each earthquake contributes to the total postseismic deformation observed at time t_i.

3. Result and Discussion

3.1. Visualization of Daily Solution Outputs from SuGAr Observations

This study utilizes the MATLAB Online platform to process daily solution data from each SuGAr observation station. The processing yields displacement time series that represent the temporal evolution of station positions, allowing detailed tracking of crustal movement across Sumatra Island. The dataset covers the period from 2002 to 2023, encompassing multiple earthquake cycles and capturing key deformation phases: preseismic, coseismic, and postseismic.

The resulting time series reveals consistent daily coordinate variations, with clear patterns of long-term tectonic motion and transient changes associated with seismic events. Notably, several stations exhibit abrupt shifts in position indicative of coseismic displacement followed by gradual postseismic deformation. These variations highlight the influence of earthquakes on surface displacement trends, demonstrating how seismic events can alter the velocity and direction of station movement over time. Time series data from eight continuous SuGAr stations (ABGS, BSAT, BTHL, BUKT, JMBI, MSAI, NGNG, and PTLO) provide insights into the complex crustal deformation along the western coast of Sumatra (Figure 2). The station exhibits predominantly linear trends in the Easting (E) and Northing (N) components, consistent with interseismic deformation driven by the oblique convergence between the Indo-Australian and Sunda Plates. The ABGS and MGNS stations show northeastward motion, consistent with regional plate kinematics, while the JMBS station records a westward movement in the E component, which may indicate localized strain accumulation near the subduction interface.

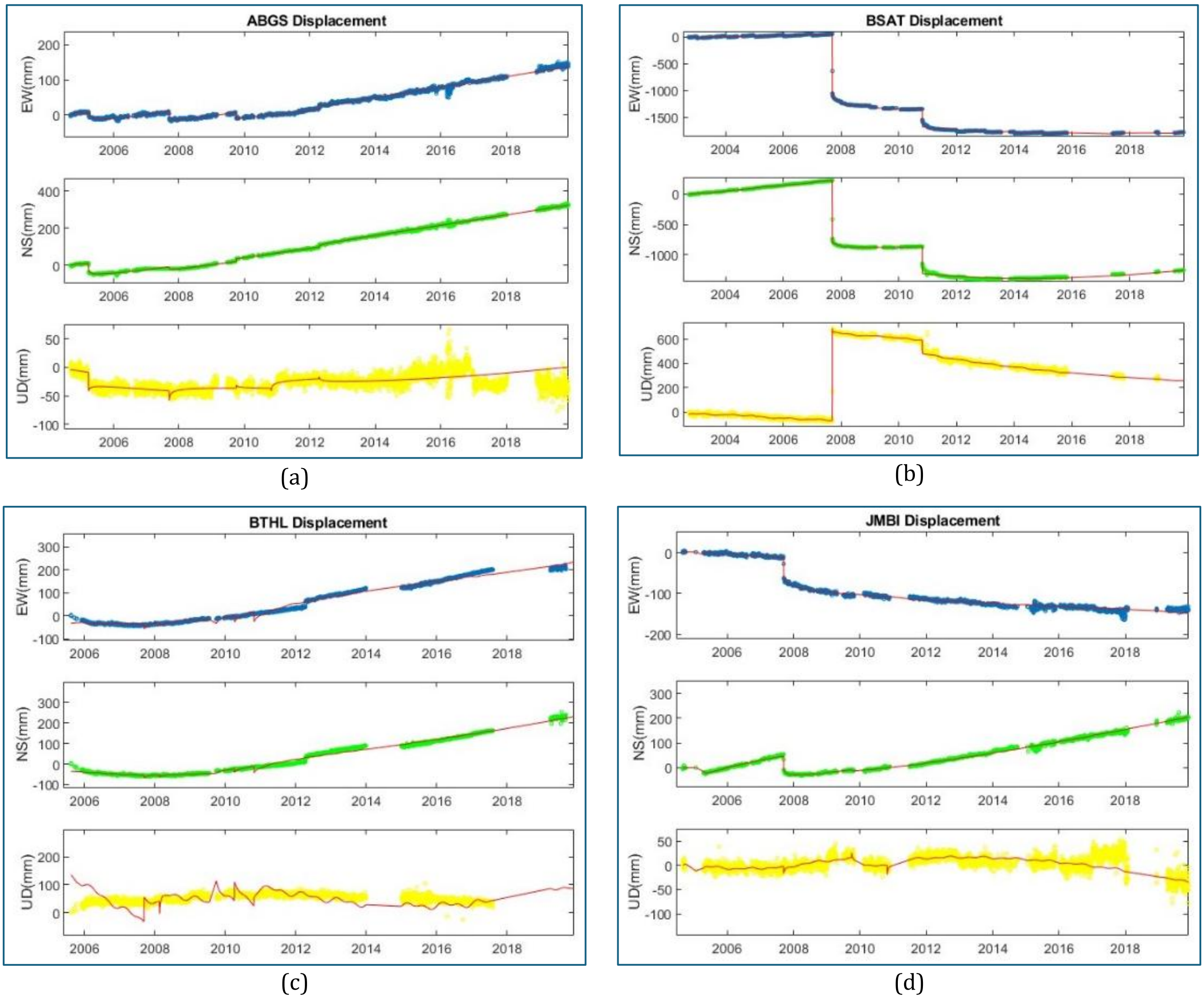

Figure 2. Daily coordinate time series of the SuGAr station (a) Station ABGS; (b) Station BSAT; (c) Station BTHL; (d) Station JMBI; (e) Station BUKT; (f) Station MSAI; (g) Station NGNG; dan (h) Station PTLO.

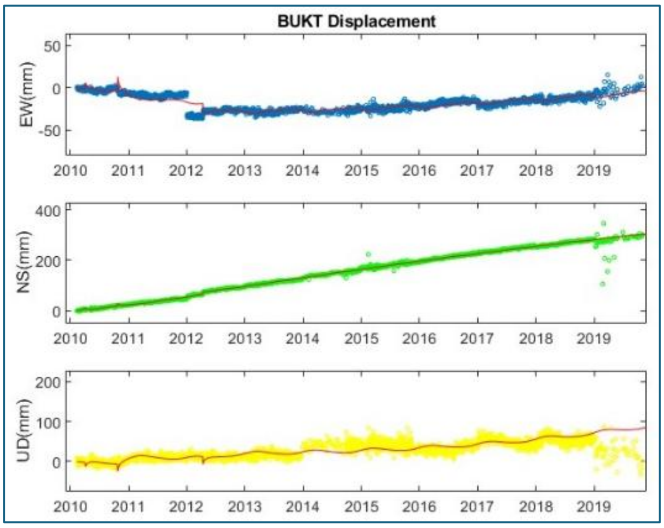

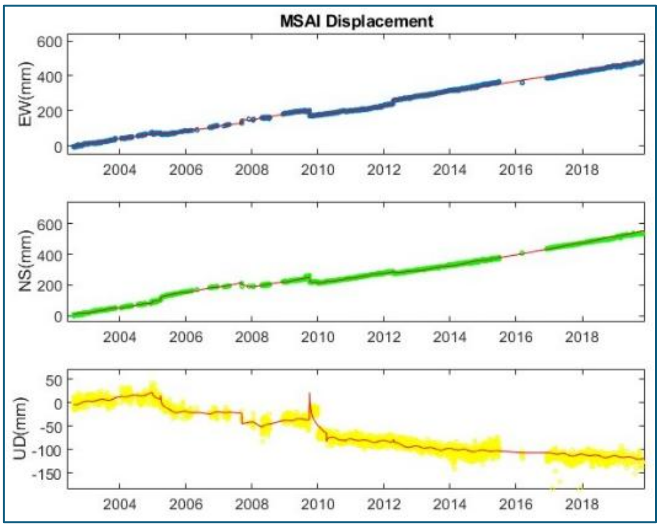

(e) (f)

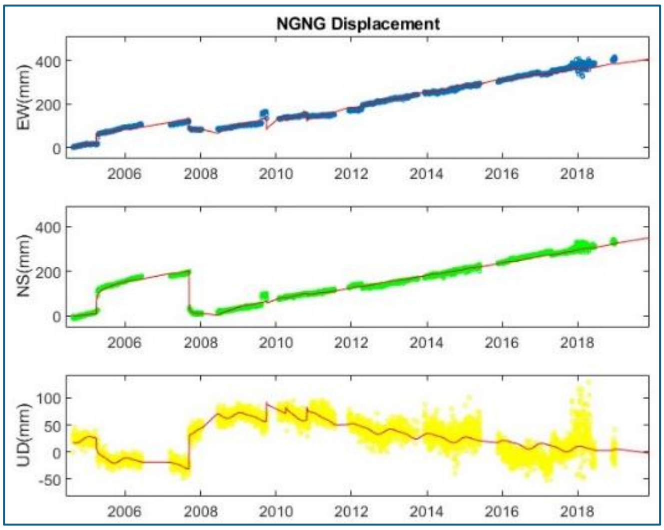

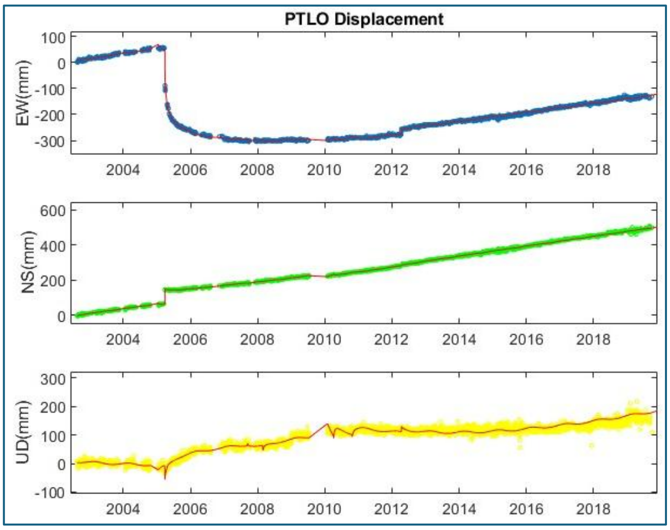

(g) (h)

Figure 2. (Continued) Daily coordinate time series of the SuGAr station (a) Station ABGS; (b) Station BSAT; (c) Station BTHL; (d) Station JMBI; (e) Station BUKT; (f) Station MSAI; (g) Station NGNG; dan (h) Station PTLO.

Postseismic deformation is evident at several stations, particularly the BTSL station, which exhibited a reversal in horizontal motion around 2010, likely associated with viscoelastic relaxation following a major earthquake. The JMBI station shows significant offsets in all three components between 2009 and 2010, consistent with a large coseismic displacement event. The MGNS station reveals intermittent gaps, which may be due to instrumental outages or site-specific challenges that hinder continuous data acquisition.

The vertical component at all stations is notably noisier than the horizontal components, reflecting common limitations in vertical GNSS positioning due to atmospheric delays and multipath effects. Nevertheless, the ABGS and MGNS stations indicate slight uplift trends, while the BTSL and JMBS stations exhibit mild subsidence. These trends, however, should be interpreted with caution due to the relatively higher uncertainty in vertical data. Seasonal signals are not prominent in the residuals, possibly because their amplitudes are low or because they are effectively modelled using annual and semiannual sinusoidal terms.

In contrast, the BSAT station records substantial coseismic displacements in all components around late 2007, most likely related to the 2007 Bengkulu earthquake. The site experienced abrupt westward and southward horizontal motion, accompanied by over 80 cm of vertical subsidence, indicative of significant elastic deformation. A slower postseismic trend is observed afterward, suggesting ongoing viscoelastic adjustment.

Overall, the GPS time series from these stations capture a combination of interseismic loading, coseismic rupture, and postseismic relaxation processes. These observations contribute to a better understanding of the active tectonic behavior in western Sumatra and can inform future efforts in seismic hazard assessment and deformation modelling. Integration with seismic catalogs and numerical models would further enhance the interpretation of crustal dynamics in this region.

3.2. Postseismic Phase Decomposition Using Exponential Approach

Earthquakes release energy as seismic waves and generate long-lasting deformation that can persist for months or even years after the mainshock. This period, known as the postseismic phase, reflects the Earth's crustal response to stress redistribution following the rupture. Postseismic deformation is typically governed by three dominant mechanisms: afterslip, viscoelastic relaxation, and their combination, each operating over different temporal and spatial scales. These mechanisms are mathematically characterized by distinct functional forms: afterslip is generally modelled using a logarithmic function of time, while viscoelastic relaxation is represented by an exponential decay. When both mechanisms are present, a superposition of the two functions is used to better describe the postseismic displacement behavior.

Accurate modelling of the postseismic phase is essential for understanding crustal deformation processes and the timescales over which the lithosphere adjusts after major seismic events. In this study, postseismic deformation is analyzed by decomposing GPS-derived displacement time series using an exponential-decay model. This approach assumes that the deformation rate decreases exponentially with time following the earthquake, capturing the characteristic behavior of viscoelastic relaxation and, to some extent, afterslip. The exponential model provides a mathematically robust framework for estimating key parameters, such as the decay time constant and postseismic velocity, which are critical for quantifying the temporal evolution of the deformation.

The decay of postseismic energy induces measurable surface deformation, often governed by viscoelastic processes in the lower crust and upper mantle. The viscoelastic mechanism is particularly effective in explaining long-term postseismic signals and is conceptually analogous to slip distribution at depth along a fault plane. To investigate this mechanism, daily GPS displacement time series were processed by removing outliers and isolating the postseismic signals. The resulting data were then fitted with an exponential function to extract the dominant decay characteristics.

The exponential decay parameter obtained from the model is defined as the time required for approximately two-thirds of the total postseismic displacement to occur, serving as a proxy for energy dissipation. Each GPS station was modelled independently, using a consistent functional form while accounting for the number and timing of earthquakes affecting each station. The estimated decay times exhibit considerable variability across stations and seismic events, highlighting the heterogeneous nature of postseismic deformation and the influence of local crustal and lithospheric properties.

Table 3. The average decay time of each earthquake based on exponential fitting

Earthquake ID	**Average R Value (Year)**		
	R_{NS}	**R_{EW}**	**R_{UD}**
1	No Stations are Affected by the Earthquake		
2			
3			
4	5.43	4.95	6.05
5	4.26	4.56	5.92
6	No Stations are Affected by the Earthquake		
7	6.67	6.63	5.19
8	5.36	5.86	6.15
9	3.21	2.39	2.39
10	5.30	4.46	5.75
11	5.04	5.15	5.22
12	No Stations are Affected by the Earthquake		
13	5.17	5.58	4.99
14	4.44	5.35	4.29
15	No Stations are Affected by the Earthquake		
16	4.65	5.26	5.01
17	4.46	5.39	4.69
18	4.64	6.18	5.93
19	No Stations are Affected by the Earthquake		
20			
21	5.48	5.48	5.54
22	No Stations are Affected by the Earthquake		
23			
24	5.67	5.57	5.57

The estimated decay times (R) vary considerably among stations and earthquake events. As shown in Table 3, some stations exhibit short decay times, indicating rapid postseismic relaxation immediately after the earthquake, whereas others exhibit longer decay times that may persist for several months. This variability reflects the heterogeneous characteristics of postseismic processes in Sumatra, including differences in fault geometry, lithospheric properties, stress redistribution, and local geological conditions.

Earthquake ID 11 shows decay times consistently recorded above five years across all directional components. A similar pattern is also observed in earthquake ID 7, where the decay time approaches 6 years, especially in the NS component. In contrast, earthquake ID

14 exhibits a different pattern, with decay times tending to be lower. Meanwhile, earthquake ID 18 shows significant fluctuations both between stations and among components.

Based on the decay times obtained using the exponential approach, earthquakes with IDs 11, 13, and 16 appear to be the strongest or most impactful events at each observation station. Conversely, ID 14 shows relatively smaller decay times, indicating a lower influence of the earthquake on the observation stations. The deformation patterns detected at each station from the exponential modelling show movement in each observation component with varying directions. Model accuracy is evaluated against observational data at each component and station using RMSE values. This evaluation aims to assess the quality of the modelling and to understand the characteristics of post-earthquake deformation directions within each observation component.

The analysis is further conducted by considering two components: the horizontal component and the three-dimensional (3D) component. The horizontal component represents the residual error magnitude solely in the horizontal movement directions, specifically the NS and EW axes. In contrast, the 3D component characterizes the direction of station movement by accounting for both horizontal and vertical axes.

Table 4. The RMSE values obtained from the processing using exponential fitting

Station	RMSE (mm)				
	NS	EW	UD	*Hori-zontal*	3D
ABGS	12.77	26.89	17.14	39.66	56.81
BSAT	7.60	7.80	64.37	15.41	79.78
BTHL	7.42	8.32	17.55	15.74	33.29
BUKT	6.82	3.65	16.63	10.47	27.10
JMBI	4.70	3.53	13.88	8.24	22.11
MSAI	10.15	6.19	16.78	16.34	33.12
NGNG	9.29	8.63	18.86	17.91	36.77
PTLO	3.85	4.86	13.97	8.71	22.68

Table 4 shows that the exponential model generally performs better for the horizontal components (NS and EW) than for the vertical (UD) component. Most stations exhibit lower RMSE values in the horizontal direction, indicating that horizontal postseismic deformation is more consistently captured by the model.

The JMBI and PTLO stations show the lowest horizontal RMSE values, suggesting good agreement between the modelled and observed displacements. In contrast, the BSAT station has the highest UD RMSE (64.37 mm), resulting in the largest 3D RMSE, indicating greater uncertainty in modelling vertical deformation. Overall, the variability of RMSE values reflects differences in local deformation characteristics and station responses to seismic events.

The RMSE values presented in Table 4 are further illustrated in the graph shown in **Error! Reference source not found.** to depict the pattern of RMSE variations across all components.

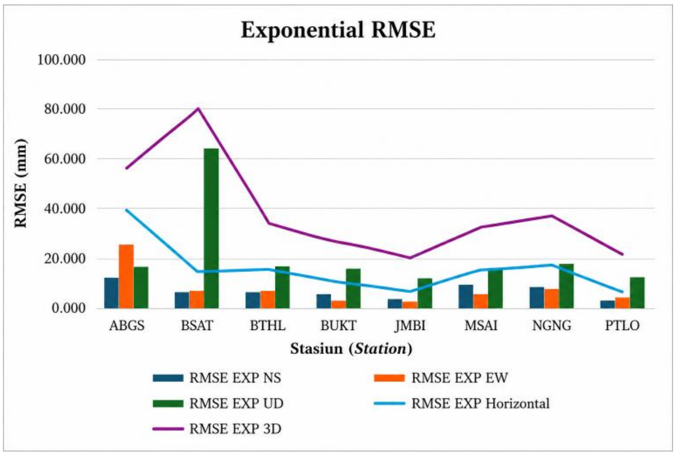

Figure 3. The variation of RMSE values for observation stations based on exponential fitting

4. Conclusion

This study demonstrates that exponential fitting can be effectively applied to decompose and characterize postseismic deformation signals from GPS displacement time series. The results indicate that the model successfully captures horizontal postseismic components, as shown by consistent decay times and relatively low RMSE values in the NS and EW directions. In contrast, the vertical component shows higher RMSE values, reflecting greater uncertainty and complexity in isolating vertical postseismic signals.

The variability in decay times across earthquakes and stations highlights the heterogeneous nature of postseismic processes, influenced by local geological conditions and source characteristics. Overall, the findings confirm that exponential-based decomposition provides a useful framework for analyzing postseismic deformation, while also emphasizing the need for complementary approaches to better resolve vertical displacement behavior.

5. Conflict of Interest Statement

The authors declare that they have no conflicts of interest regarding the research, authorship, or publication of this article.

6. Reference

DeMets, C., Gordon, R. G., & Argus, D. F. (2010). Geologically current plate motions. Geophysical Journal International, 181(1), 1–80. https://doi.org/10.1111/j.1365-246X.2009.04491.x

Deo, M. N., Zhang, K., Roberts, C., & Talbot, N. C. (2003). *An investigation of GPS precise point positioning methods*. In *Proceedings of the 6th International Symposium on Satellite Navigation Technology Including Mobile Positioning & Location Services*. Melbourne, Australia.

Diao, F., Wang, R., Wang, Y., Xiong, X., & Walter, T. R. (2018). Fault behavior and lower crustal rheology inferred from the first seven years of postseismic GPS data after the 2008 Wenchuan earthquake. *Earth and Planetary Science Letters, 495*, 202–212. https://doi.org/10.1016/j.epsl.2018.05.020

Emry, E. L., Wiens, D. A., & Garcia-Castellanos, D. (2014). Faulting within the Pacific plate at the Mariana Trench: Implications for plate interface coupling and subduction of hydrous minerals. *Journal of Geophysical Research: Solid Earth*, *119*(4), 3076–3095.

Feng, L., Hill, E. M., Banerjee, P., Hermawan, I., Tsang, L. L. H., Natawidjaja, D. H., Suwargadi, B. W., & Sieh, K. (2015). A unified GPS-based earthquake catalog for the Sumatran plate boundary between 2002 and 2013. Journal of Geophysical Research: Solid Earth, 120(5), 3566–3598. https://doi.org/10.1002/2014JB011661

Fialko, Y. (2004). Probing the mechanical properties of seismically active crust with space geodesy: Study of the coseismic deformation due to the 1992 Mw 7.3 Landers (Southern California) earthquake. *Journal of Geophysical Research: Solid Earth*, *109*(B3).

Hall, R., & Spakman, W. (2015). Mantle structure and tectonic history of SE Asia. *Tectonophysics*, *658*, 14–45. https://doi.org/10.1016/j.tecto.2015.07.003

Holden, L., Silcock, D., Choy, S., Cas, R., Ailleres, L., & Fournier, N. (2017). Evaluating a campaign GNSS velocity field derived from an online precise point positioning service. *Geophysical Journal International*, *208*(1), 246–256. https://doi.org/10.1093/gji/ggw372

Kreemer, C., Blewitt, G., & Maerten, F. (2006). Co- and postseismic deformation of the 28 March 2005 Nias Mw 8.7 earthquake from continuous GPS data. *Geophysical Research Letters*, *33*(7). https://doi.org/10.1029/2005GL025566

Li, X., Ge, M., Zhang, X., Zhang, Y., Guo, B., Wang, R., Klotz, J., & Wickert, J. (2013). Real-time high-rate co-seismic displacement from ambiguity-fixed precise point 120 positioning: Application to earthquake early warning. Geophysical Research Letters, 40(2), 295–300. https://doi.org/10.1002/grl.50138

Pratama, C., Susanta, F. F., Ilahi, R., Khomaini, A. F., & Abdillah, H. W. K. (2019). Coseismic displacement accumulation between 1996 and 2019 using a global empirical law on Indonesia continuously operating reference station (InaCORS). JGISE: Journal of Geospatial Information Science and Engineering, 2(2), 237–244. https://doi.org/10.22146/jgise.51130

Pratama, C., Meilano, I., Sunarti, E., Haksama, S., & Sulistiyo, M. D. (2020). Data-driven time series decomposition for estimating geodetic secular motion around the Palu-Koro Fault Zone. 2020 8th International Conference on Information and Communication Technology (ICoICT). https://doi.org/10.1109/ICoICT49345.2020.9166422

Wang, H., Liu, M., Shen, X., & Liu, J. (2010). Balance of seismic moment in the Songpan-Ganze region, eastern Tibet: Implications for the 2008 Great Wenchuan earthquake. Tectonophysics, 491(1–4), 154–164. https://doi.org/10.1016/j.tecto.2009.09.022

Yusiyanti, I., Khasanah, F. A., Trihandaru, K. R., Kalbuadi Prajardi, T. W., Pratama, C., & Wibowo, S. T. (2023). Vertical deformation model on postseismic phase using exponential approach: A case study of the 2018 Palu earthquake. Geodesy and Geodynamics, 14(2), 123–134. https://doi.org/10.1016/j.geog.2023.01.003

Yusiyanti, I., Khasanah, F. A., Trihandaru, K. R., Kalbuadi Prajardi, T. W., Pratama, C., & Wibowo, S. T. (2025). Spatiotemporal postseismic deformation due to the 2018 Palu-Donggala earthquake revealed the relative importance of viscoelastic relaxation and afterslip distribution estimated from geodetic observations. Journal of Applied Geodesy. https://doi.org/10.1515/jag-2024-0017